Environ Monit Assess _####################_
https://doi.org/10.1007/s10661-018-6921-y

Land consumption monitoring: an innovative method integrating SAR and optical data

Sara Mastrorosa · Michele Crosetto · Luca Congedo · Michele Munafò

Received: 2 February 2018 / Accepted: 14 August 2018

Abstract In this paper, the use of synthetic aperture radar (SAR) for the monitoring of land consumption is analyzed. The paper presents an automatic procedure that integrates SAR and optical data, which can be effectively used to generate land consumption maps or update existing maps. The main input of the procedure is a series of SAR amplitude images acquired over a given geographical area and observation period. The main assumption of the procedure is that land consumption is associated with an increase of the SAR amplitude values. Such an increase is detected in the SAR amplitude time series using an automatic Bayesian algorithm. The results based on the SAR amplitude are then filtered using an NDVI map derived from optical imagery. The effectiveness of the proposed procedure is illustrated using SAR data from the Sentinel-1 and TerraSAR-X sensors, and optical data from the Sentinel-2 sensor.

Keywords Multi-temporal series · SAR images · Step detection · Time series · Land use/land cover

S. Mastrorosa (✉)
Civil and Environmental Engineer, Via Serra De'Conti 68, 00138 Rome, Italy
e-mail: saramastrorosa@gmail.com

M. Crosetto
Geomatics Division Head, Remote Sensing Department, Centre Tecnològic de Telecomunicacions de Catalunya (CTTC), Barcelona, Spain

L. Congedo · M. Munafò
ISPRA - Italian Institute for Environmental Protection and Research, Rome, Italy

Introduction

Land consumption is a phenomenon associated with the loss of an important environmental resource: agricultural, natural, or semi-natural land. The phenomenon refers to an increase of the artificial covering of the ground, due to settlement dynamics. It is defined as a change from a non-artificial covering (unconsumed land) to an artificial covering of the soil (consumed land) (EEA 2011; ISPRA 2017). It is a process that is mostly attributable to settlements, expansion of cities, construction of new buildings and infrastructures, densification of urban areas, etc. (Scalenghe and Ajmone Marsan 2009).

At the European level, land consumption is a major issue that urged the European Commission to publish the guidelines on best practice to limit, mitigate, or compensate soil sealing (European Commission 2012) in order to reduce land consumption and land cover change.

It is worth highlighting that soil sealing, soil consumption, and land consumption are highly interrelated (Huber et al. 2008).

Excessive land consumption has several consequences, namely, contamination, erosion, hydrologic cycle alteration, impact on historical, cultural and landscape heritage, loss of the ability to produce raw materials, scenic pollution, degradation of the landscape, etc. (Scalenghe and Ajmone Marsan 2009; Munafò and Riitano 2016). For this reason, it is important to monitor the evolution of land use and cover, and in particular land consumption, to preserve natural and non-renewable sources.

Land cover monitoring is useful for assessing ecosystem services and supporting decision making (Maes et al. 2012).

The monitoring of impervious surfaces using remote sensing can be reliable and affordable (Fan, Wen, and Wang Fan et al. 2007; Brook and Davila Brook and D ávila 2000). The characteristics of remote sensing data such as the reference system, classification system, and legend are fundamental for monitoring land consumption (CRCS 2012).

Different are the conventional methods for land consumption monitoring. Some of the existing methods are based on a mix of semi-automatic classification (Estoque et al. Estoquea et al. 2015) and photointerpretation of satellite and airborne optical images (Munafò et al. 2016; Gómez et al. 2016), whereas others on spectral indices (Sun et al. 2017; As-syakur et al. 2012).

Although optical remote sensing is a powerful input for land consumption management tools (Congedo et al. 2017; Gómez et al. 2016), it suffers from some limitations, the most relevant being that the images can only be used under cloud-free sky conditions. An alternative to optical remote sensing is the use of synthetic aperture radar (SAR) imagery (Moran et al. 2002; Gomez-Chova et al. 2006). SAR imagery can be acquired day and night and in any weather conditions. It is particularly useful for monitoring areas of the globe where cloud cover is almost permanent and optical images are unusable (Campbell and Wynne 2011; Zhu Z. et al. Zhu et al. 2012).

SAR sensors can obtain information about the ground on a frequent basis. This permits the monitoring of rapid land use changes and urban development, providing useful information for land use planning. For example, JERS-1 SAR series images were used to analyze land use changes (Angelis et al. 2002), and COSMO-Skymed data were used for land cover classification (Satalino et al. 2011). Other works include an unsupervised change detection (Yousif and Ban 2015), a soil moisture retrieval (Zhang et al. 2018), or the analysis of natural hazards (Poursanidis et al. Poursanidis and Chrysoulakis 2017).

To date, land consumption mapping is mostly done through the assistance of an operator capable of recognizing the transformations that have taken place (Lam 2008; Congedo et al. 2017). This requires a time-consuming and expensive procedure. For this reason, it is important to implement automatic methods to expedite land consumption mapping and reduce costs.

In this work, we propose an automated procedure based on the use of multi-temporal SAR data. The developed algorithm relies on the principle that artificial structures reflect more than natural soil or vegetation; therefore, when they are built, they cause abrupt changes in the SAR amplitude. The procedure makes use of an automatic step detection algorithm, which is based on a Bayesian approach, and which is run on SAR amplitude image time series.

Two types of SAR data were used in this study: Sentinel-1 images covering two test areas (Barcelona and Rome) and TerraSAR-X images covering the area of Barcelona. The use of Sentinel-1 imagery is preferred for its continuous and systematic mapping over wide areas, and for the fact that Sentinel-1 images are free of charge: this is an important advantage for the implementation of the procedure.

Proposed procedure

The proposed method requires a time series of SAR images, i.e., a temporal series of SAR images relative to the same area. The higher the resolution of these images, the better the obtained results will be. Let us consider N co-registered SAR amplitude images. The goal of the procedure is to identify abrupt changes in the amplitude values (amplitude steps), which can be due to anthropogenic activity. Among the various existing algorithms that may be used to derive the presence of steps within time series, in this work, we have chosen a step detection algorithm based on a Bayesian approach (O'Ruanaidh and Fitzgerald 1996).

Step detector algorithm

The algorithm assumes that there is at most one single step in a given time series. The step can be modeled as follows (O'Ruanaidh and Fitzgerald 1996):

$$d_i = \begin{cases} d_1 = \mu_1 + n_1(i) & if \quad i \le m \\ d_2 = \mu_2 + n_2(i) & if \quad m+1 \le i \le N \end{cases} \tag{1}$$

where d_i represents the amplitude value under analysis, μ_1 and μ_2 are two constant amplitudes, $n_1(i)$ and $n_2(i)$ are the additive white Gaussian noise, N is the length of the time series, and m is the position of the step in the time series.

The likelihood function is given by the probability:

$$p(d|\theta,I) = \prod_{i=1}^{m} p(d_1(i)) \cdot \prod_{i=m+1}^{N} p(d_2(i)) \quad (2)$$

Where θ is a set of values assumed by the signal parameters $\{\mu_1, \mu_2, \sigma_1, \sigma_2, m\}$, σ_1 and σ_2 are the standard deviations of noise samples, and I denotes the set of a priori information available or the assumptions that have led to model the signal in this way.

According to Bayes' Theorem:

$$p(\theta|d,I) = \frac{p(\theta|I)\cdot p(d|\theta,I)}{p(d|I)} \quad (3)$$

The probability of the model θ given the data (e.g., the posterior distribution) equals the prior distribution of the model, multiplied by the probability of the data given the model (e.g., the likelihood which refers to past events that provided known results and is the direct problem), divided by the prior distribution of the data.

O'Ruanaidh and Fitzgerald (1996) demonstrate that the probability density ($p(\theta|\, d,\, I)$) can be expressed as follows:

$$p(\theta|d,I) \propto \frac{1}{\sqrt{m\cdot(N-m)}} \cdot \left[\sum_{i=1}^{m} d_i^2 - \frac{1}{m}\left(\sum_{i=1}^{m} d_i\right)^2\right]^{\frac{-m-2}{2}} \cdot \left[\sum_{k=m+1}^{N} d_k^2 - \frac{1}{N-m}\left(\sum_{k=m+1}^{N} d_k\right)^2\right]^{\frac{-N-m-2}{2}} \quad (4)$$

The ($p(\theta|\, d,\, I)$) is computed for each $m = 2, \ldots, N-1$. The position of the step is found in correspondence to the maximum of the ($p(\theta|\, d,\, I)$) function.

Identification of land consumption

The above-described step detector is used in this work to detect changes related to land consumption. After identifying a step with the above approach, in order to decide whether or not the given jump is significant; we apply the following empirical three-step procedure.

First of all, we only consider the maximum probabilities that are above a given threshold, which is obtained experimentally:

$$P_{\mathrm{mMAX}} > X \quad (5)$$

where P indicates the step probability value from (4), mMAX is the corresponding image index and X is the given probability threshold. If the probability is below the threshold, the candidate step is discarded. In addition, we require the probability function ($p(\theta|\, d,\, I)$) to have a peak shape around the position mMAX. This is expressed by the following inequality:

$$\frac{P_{\mathrm{mMAX}}}{(P_{\mathrm{mMAX+1}} + P_{\mathrm{mMAX-1}})/2} > Y \quad (6)$$

where mMAX + 1 and mMAX − 1 indicate the indices of the images preceding and following the maximum location mMAX, and Y is a given empirical threshold. If Eq. 6 is not satisfied, the candidate step is discarded. Finally, after selecting those pixels that comply with the previous two conditions, we force the amplitude value to increase after the jump, i.e.,

$$\mathrm{med}_{\mathrm{after\_mMAX}} - \mathrm{med}_{\mathrm{before\_mMAX}} > Z \quad (7)$$

where $\mathrm{med}_{\mathrm{after\_mMAX}}$ indicates the median of the amplitude values after the candidate step, $\mathrm{med}_{\mathrm{before\_mMAX}}$ indicates the median of the amplitude values preceding the step, and Z is a given empirically derived threshold. If the three above conditions are fulfilled, we consider that the candidate step corresponds to a potential instance of land consumption. The procedure is run for all the pixels of the study area. This is followed by data geocoding and the integration with optical data. The final step is the validation of the automatically derived results by photointerpretation.

Output of the method

The automatic detection procedure described above generates a three-class map:

- *Class = 0*: There is no detected change;
- *Class = 1*: A transformation occurred, but it cannot be attributed to land use consumption;
- *Class = 2*: A change occurred, which can be attributed to land consumption.

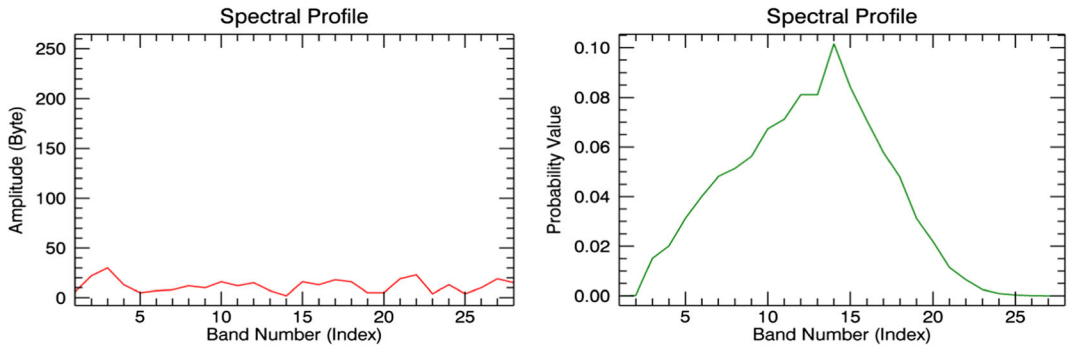

Fig. 1 Example of class 0. Amplitude time series (left) and the corresponding probability function (right)

Figure 1 shows an example of class 0. From the amplitude time series, it is evident that there is no change. The probability function shows a low probability maximum (0.10). An example of class 1 is shown in Fig. 2. In this case, there is a clear amplitude jump, but it cannot be attributed to land consumption because it corresponds to a decrease of the amplitude values. It represents an opposite phenomenon: from soil sealing to agricultural/forest. Another example of class 1 is shown in Fig.

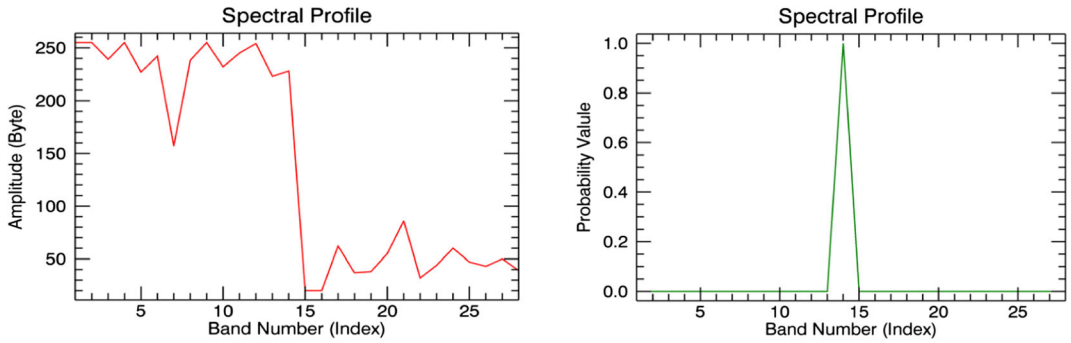

Fig. 2 Example of class 1. Amplitude time series (left) and the corresponding probability function (right)

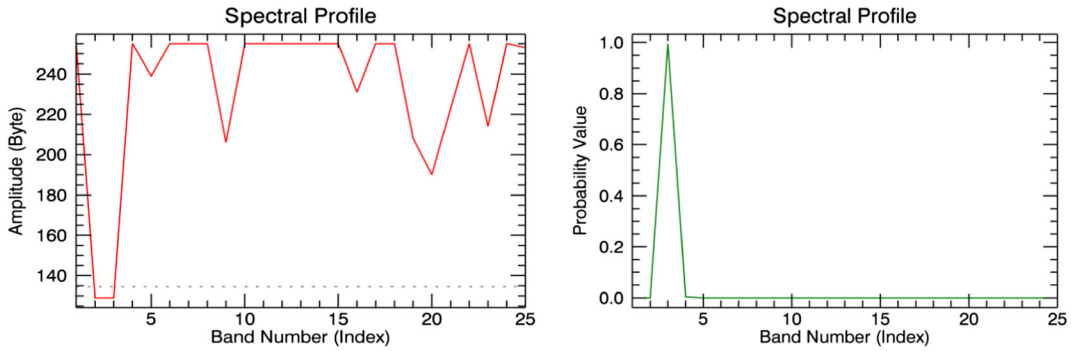

Fig. 3 Example of class 1. Amplitude time series (left) and the corresponding probability function (right)

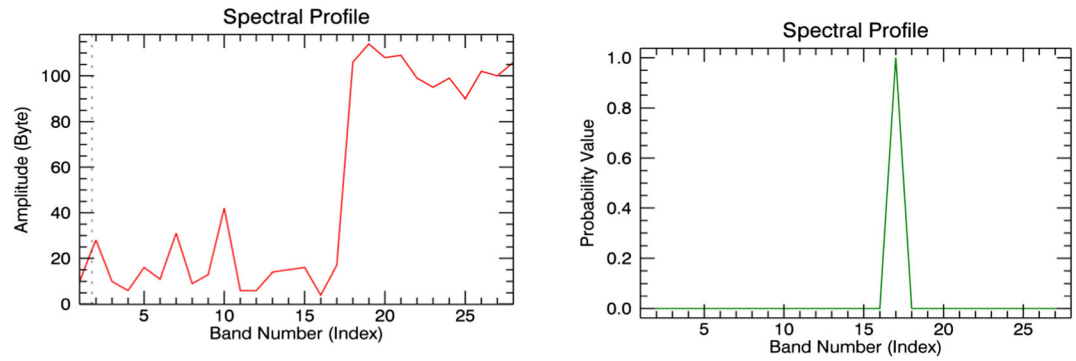

Fig. 4 Example of class 2. Amplitude time series (left) and the corresponding probability function (right)

3. In this case, the candidate step seems to be due to two anomalous amplitude values, and not to land consumption. Finally, Fig. 4 shows an example of class 2, where there is a clear jump, associated with an increase of the amplitude values.

To illustrate the proposed algorithm, Fig. 5 shows the proposed classification method through an algorithm flowchart.

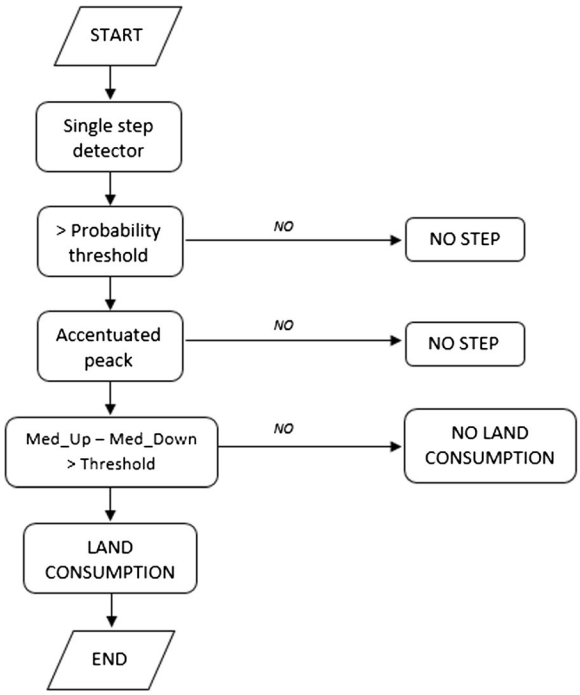

Fig. 5 Schematic algorithm flowchart

Integration with optical data

The three-class land consumption map derived using SAR data is filtered using the information coming from optical data. These data are used to derive the NDVI map[1] relative to the period after the potential change. The basic idea is that land consumption can only occur where there is no vegetation in the above NDVI. In this way, we filter out several false land consumption cases. For this purpose, we use the following simple filter: we consider that there is correct land consumption detection if the SAR-derived class is 2 and, at the same time, the NDVI, after the potential change, is below a given threshold.

Case studies

In this section, we examine three case studies in which the above procedure was applied.

The study areas were chosen considering image availability in the two research centers involved in this work.

Barcelona case study using Sentinel-1 data

The test area covers approximately 800 km^2 (see Fig. 6). The study was based on a stack of 25 co-registered SAR amplitude images from the Sentinel 1-A satellite that cover a period of 11 months, from March 6, 2015 to February 5, 2016 (see Fig. 7). These images are

[1] The number of images to create an accurate NDVI map depends mainly on the season (vegetation phenology) and on the cloud cover. Theoretically, even one image could be enough if acquired in the season of maximum vegetation growth and with no cloud cover.

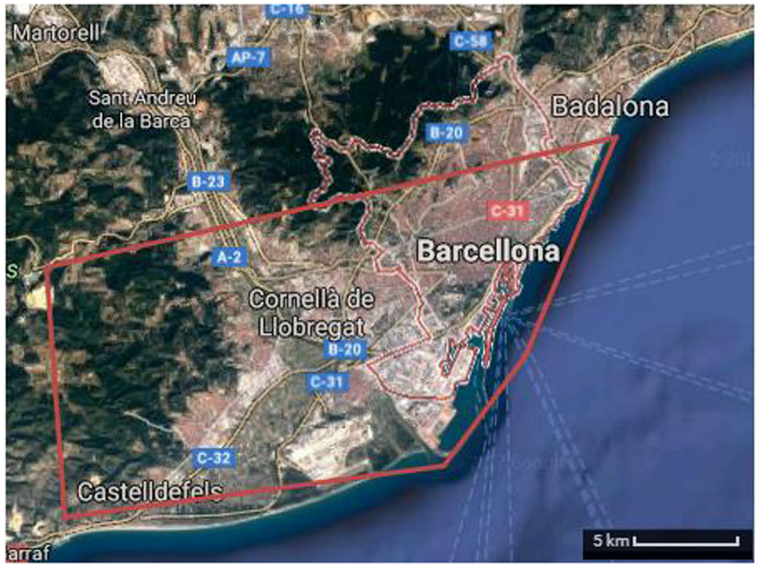

Fig. 6 Optical image of Barcelona test area, indicated by the red polygon

medium-resolution SAR images, with a ground pixel footprint of approximately 14 (range) by 5 (azimuth) m. The procedure was run setting the following empirically chosen thresholds (Eqs. 5, 6, and 7): $X = 0.75$, $Y = 30$, and $Z = 60$. The results of the classification were geocoded and compared with optical images from Google Earth.

In the entire area, 12 potential land consumption cases were detected. We briefly describe some of them. Figures 8 and 9 show some changes that occurred in the port of Barcelona. The detected changes are represented by the red pixels in the change detection maps. These changes, which cause a clear increase of the SAR amplitude, are due to the displacement of containers: this is clearly visible in the two optical images. These changes represent an example of temporary changes occurring on already-consumed land. Figures 10, 11, 12, and 13 show examples of detected land consumption. In all cases, there is a clear increase of the SAR amplitude.

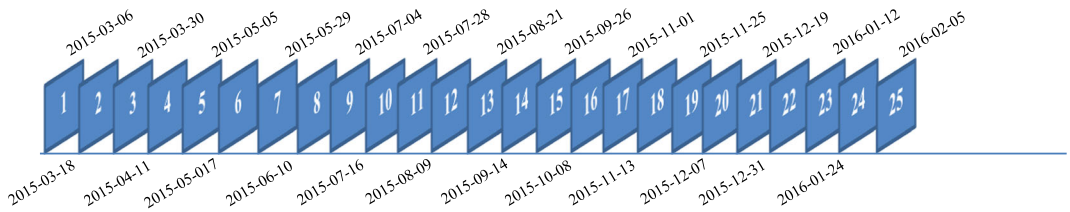

Fig. 7 Sentinel-1 images of the Barcelona case study

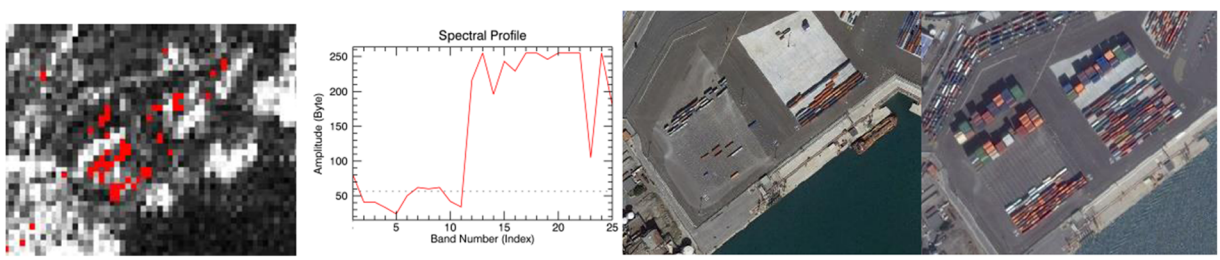

Fig. 8 Change detection map (**a**); amplitude time series (**b**); Google Earth image, March 28, 2015 (**c**); Google Earth image, November 5, 2015 (**d**)

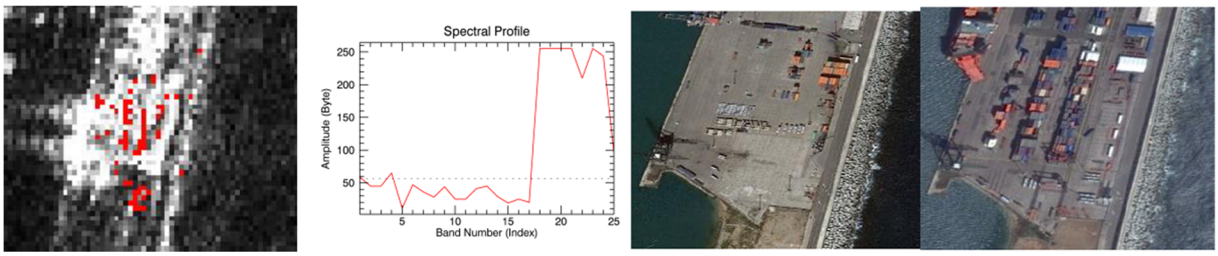

Fig. 9 Change detection map (**a**); amplitude time series (**b**); Google Earth image, March 28, 2015 (**c**); Google Earth image, April 07, 2016 (**d**)

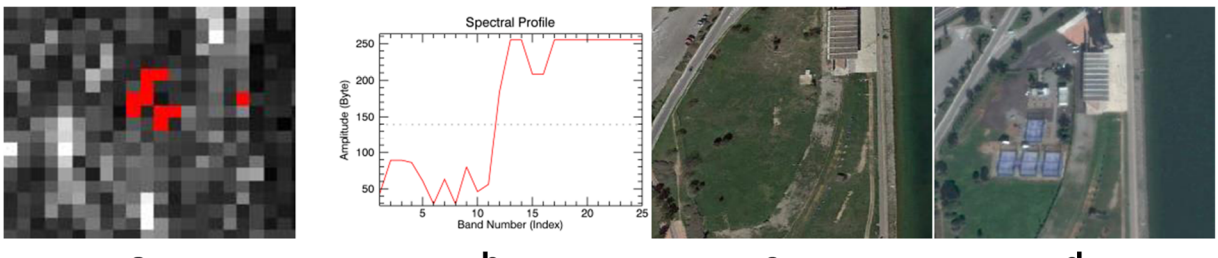

Fig. 10 Change detection map (**a**); amplitude time series (**b**); Google Earth image, March 28, 2015 (**c**); Google Earth image, November 05, 2015 (**d**)

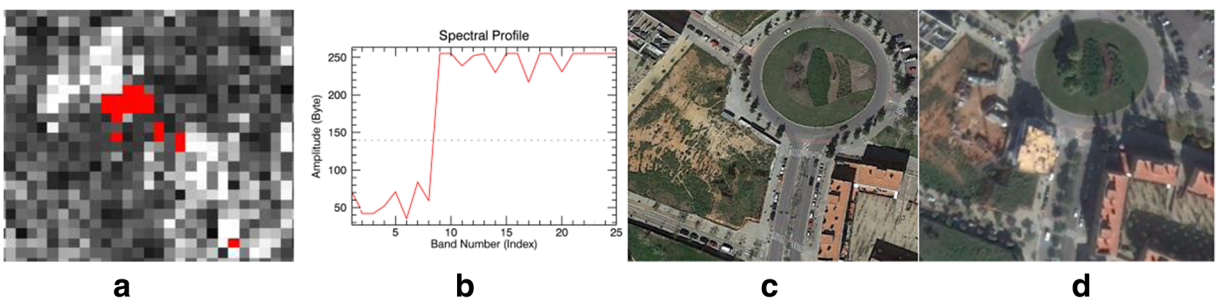

Fig. 11 Change detection map (**a**); amplitude time series (**b**); Google Earth image, March 28, 2015 (**c**); Google Earth image, November 05, 2015 (**d**)

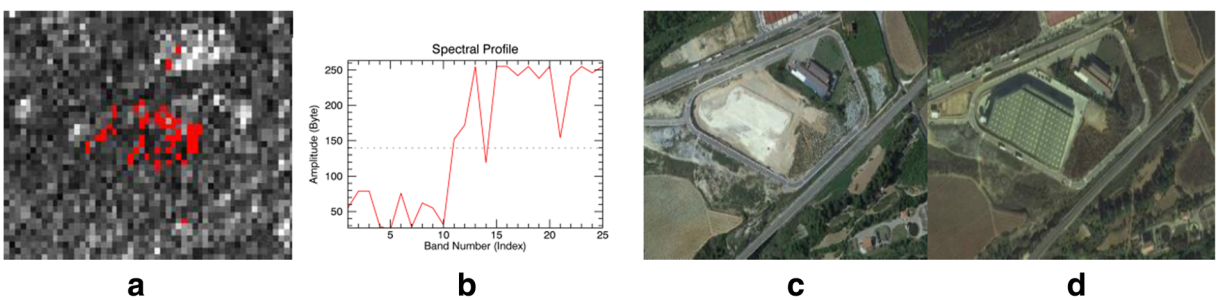

Fig. 12 Change detection map (**a**); amplitude time series (**b**); Google Earth image, March 28, 2015 (**c**); Google Earth image, November 05, 2015 (**d**)

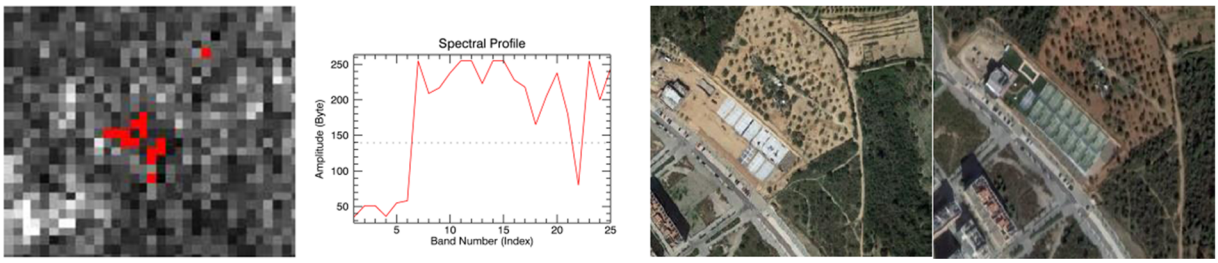

Fig. 13 Change detection map (**a**); amplitude time series (**b**); Google Earth image, March 28, 2015 (**c**); Google Earth image, November 05, 2015 (**d**)

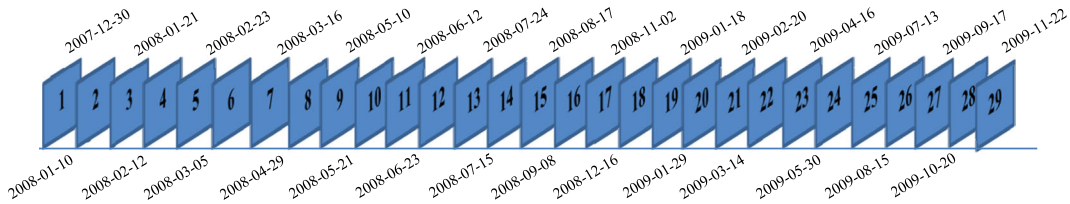

Fig. 14 TerraSAR-X images of the Barcelona case study

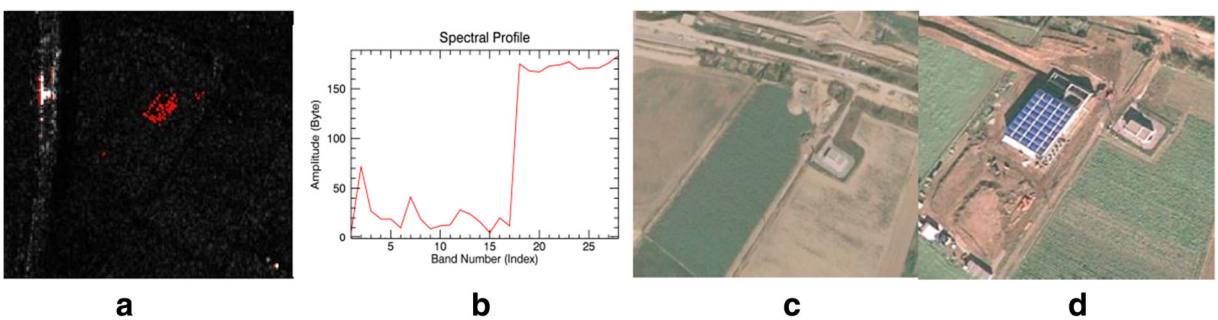

Fig. 15 Change detection map (**a**); amplitude time series (**b**); Google Earth image, December 31, 2008 (**c**); Google Earth image, April 14, 2009 (**d**)

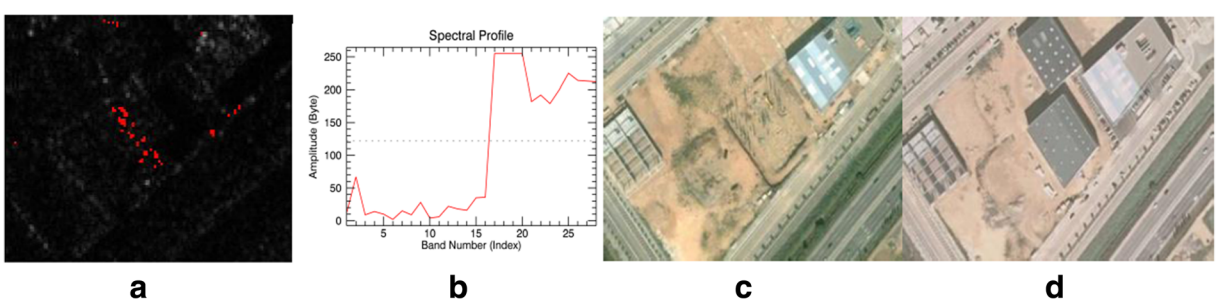

Fig. 16 Change detection map (**a**); amplitude time series (**b**); Google Earth image, September 11, 2007 (**c**); Google Earth image, December 31, 2008 (**d**)

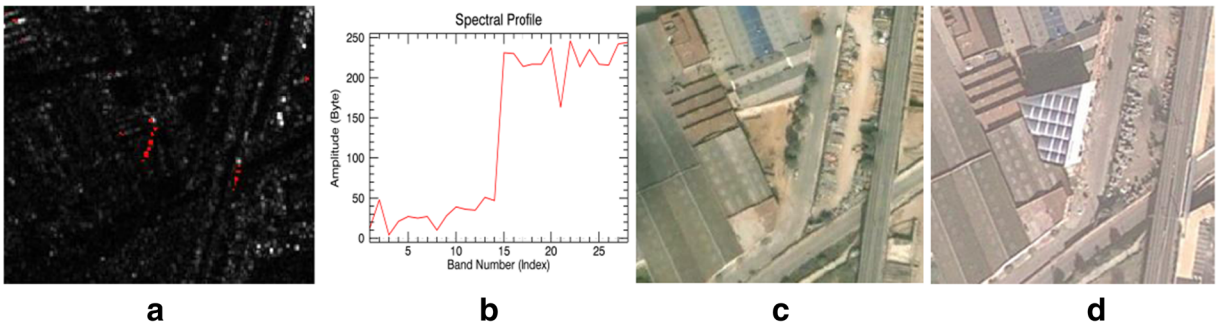

Fig. 17 Change detection map (**a**); amplitude time series (**b**); Google Earth image, November 15, 2007 (**c**); Google Earth image, February 07, 2008 (**d**)

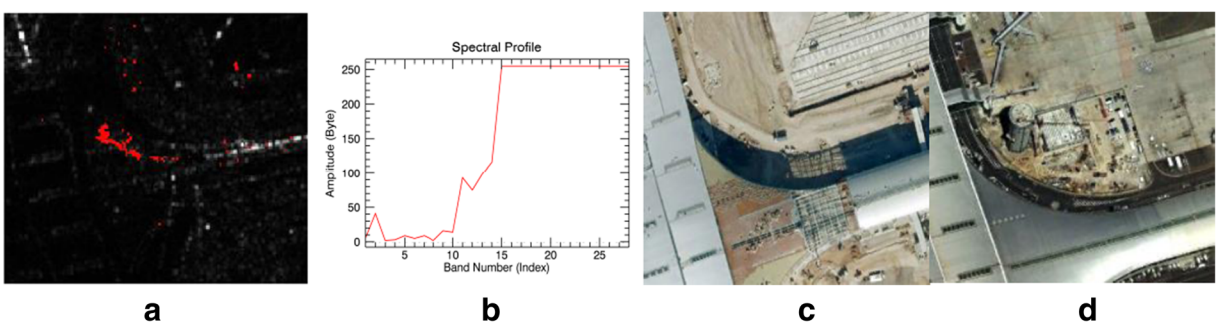

Fig. 18 Change detection map (**a**); amplitude time series (**b**); Google Earth image, November 15, 2007 (**c**); Google Earth image, April 14, 2009 (**d**)

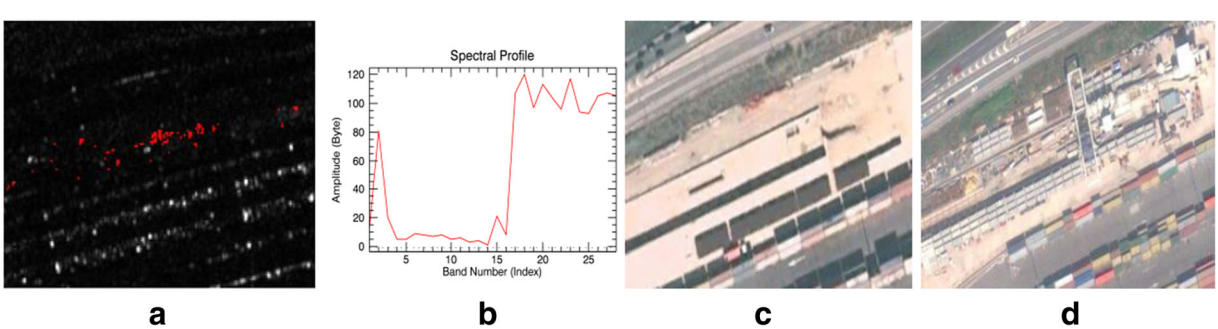

Fig. 19 Change detection map (**a**); amplitude time series (**b**); Google Earth image, December 31, 2008 (**c**); Google Earth image, February 07, 2009 (**d**)

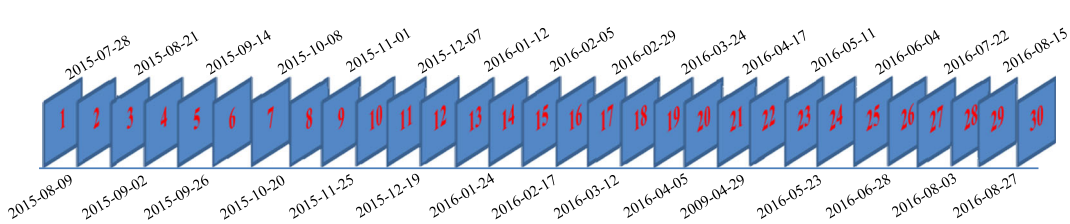

Fig. 20 Sentinel-1 images of the Rome case study

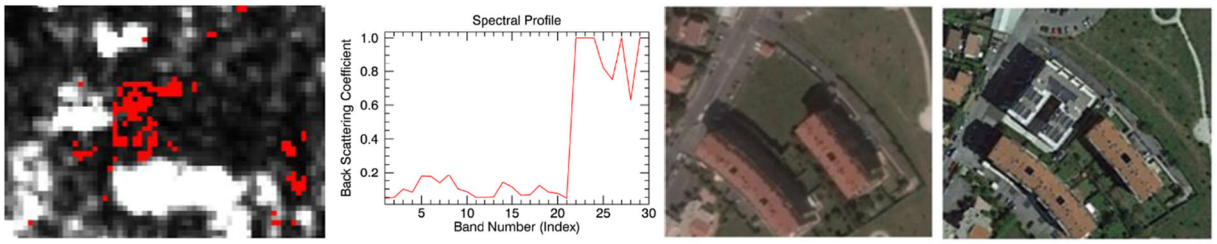

Fig. 21 Change detection map (**a**); amplitude time series (**b**); Google Earth image, July 17, 2015 (**c**); Google Earth image, October 28, 2016 (**d**)

The different types of land consumption can be highlighted from the optical images.

Barcelona case study using TerraSAR-X data

The second case study was based on 29 co-registered SAR amplitude images from the TerraSAR-X satellite that cover the period from December 30, 2007 to November 22, 2009 (see Fig. 14). Unfortunately, it was not possible to consider the same period of the first case study due to the unavailability of the images. Therefore, a direct comparison of the results of the two case studies was not possible. The images used are very high resolution, with a pixel footprint of 3 × 3 m and with less noisy amplitude time series. The covered area is 400 km^2. We run the same procedure used for the first case study, using the same thresholds: $X = 0.75$, $Y = 30$, and $Z = 60$. The results of the classification were geocoded and compared with optical images from Google Earth.

Examples of correct detection of land consumption cases are shown in Figs. 15, 16, 17, and 18. As mentioned above, the amplitude time series are less noisy than those of Sentinel-1 data. Figure 19 shows an example of change on soil already consumed (displacement of containers) or on bare soil.

Rome case study using Sentinel-1 data and Google Earth Engine

The third case study was based on 30 co-registered SAR amplitude images from the Sentinel-1 satellite that cover the period from July 28, 2015 to August 27, 2016 (see Fig. 20.). The covered area is approximately 250 km^2. In this case, the processing was done using Google Earth Engine[2] (GEE). This platform was used in different types of remote sensing studies (Patel et al. 2015; Gorelick et al. 2017).

The satellite SAR amplitude data were directly accessed using GEE. This represents a considerable advantage with respect to the traditional approach, which requires downloading the data into a local machine. The procedure was implemented in a Python programming language script. We run the same procedure used for the first two case studies, using the same thresholds: $X = 0.75$, $Y = 30$, and $Z = 60$.

Figures 21 and 22 show some of the obtained results. Figure 21 shows a broad change that takes place in the 21st image (April 17, 2016) in the area of Colle Salario (Rome). Figure 22 shows another change occurring in the area of Castel Giubileo (Rome).

In the Rome case study, the NDVI was calculated using all the Sentinel-2 images available in the temporal range March 29, 2016 to November 24, 2016 (see Fig. 23). The maximum value of the NDVI series was derived in order to exclude those pixels covered by vegetation in at least one image, enabling the masking of non-built-up pixels. The NDVI was used to filter the results based on SAR images. An example is described below.

Figure 24 shows the map of potential land consumption changes. In this map, the code 0 indicates areas where there were no land consumption changes in the studied period, whereas code 2 indicates areas where changes have potentially occurred. The map presents many isolated pixels and pixels whose position is due to temporary changes. In particular, the main red cluster is due to the presence of trucks at a warehouse. Therefore, in this case, the potential change is not related to land consumption.

The NDVI is used to filter such false land consumption detection (see Fig. 25).

The NDVI refers to the last months of the observed period. In this map, code 1 indicates areas where the value of NDVI is under a certain value (0.4 was selected

[2] The Google Earth Engine includes historical images from 1990 to date, continuously collects new images and, in addition to providing APIs (application programming interfaces) in Java Script and Python, provides useful tools for analyzing large sets of images.

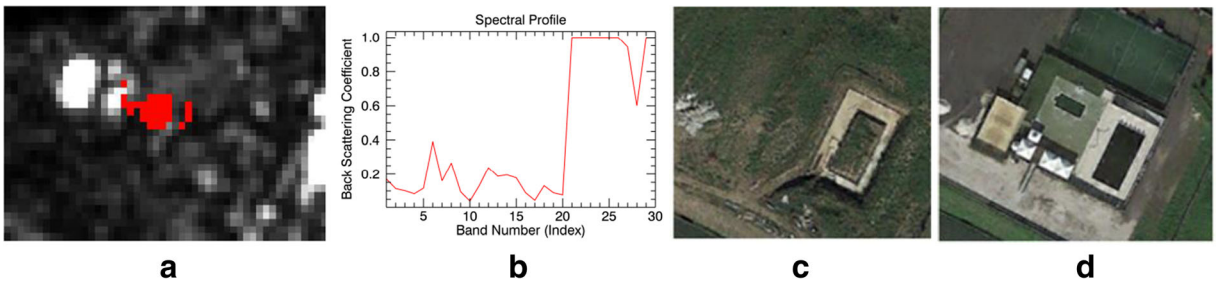

Fig. 22 Change detection map (**a**); amplitude time series (**b**); Google Earth image, July 17, 2015 (**c**); Google Earth image, October 28, 2016 (**d**)

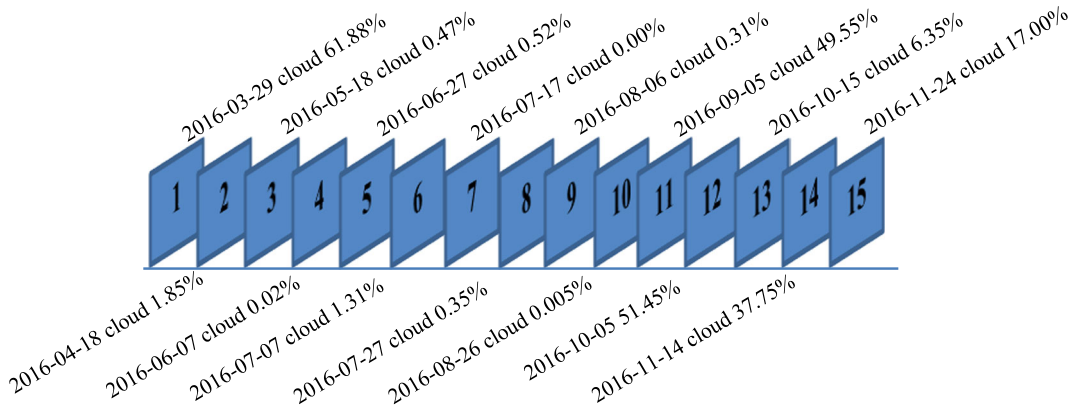

Fig. 23 Sentinel-2 images of the Rome case study

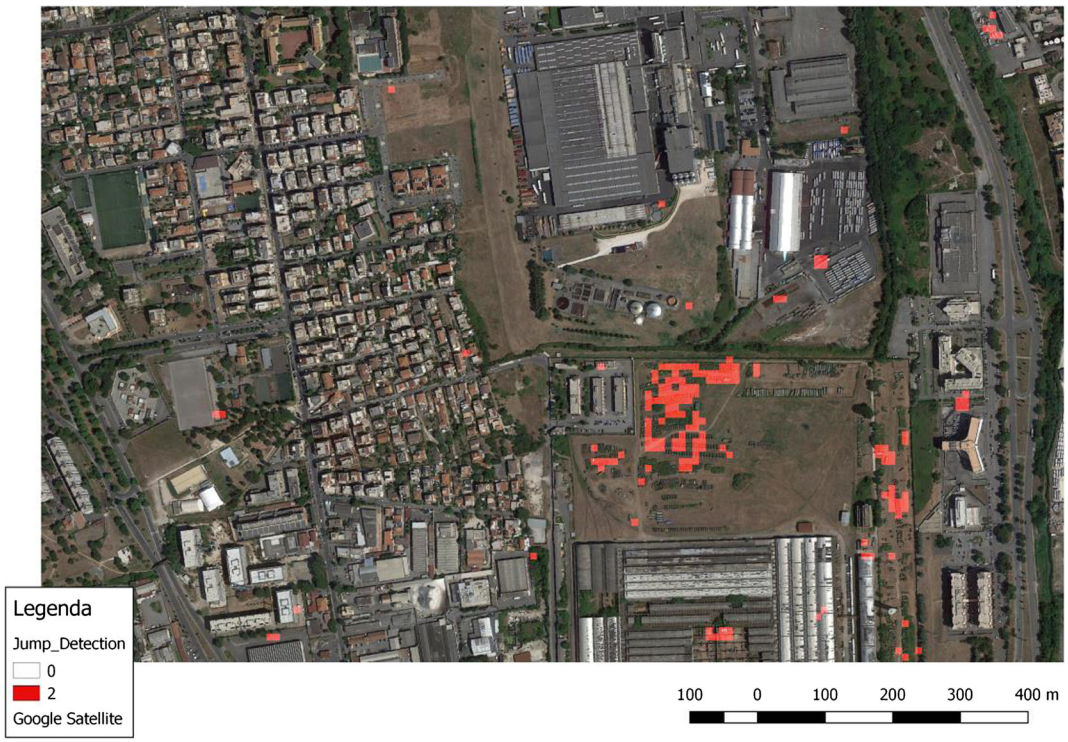

Fig. 24 Map of potential land consumption change, Colle Prenestino–Rome

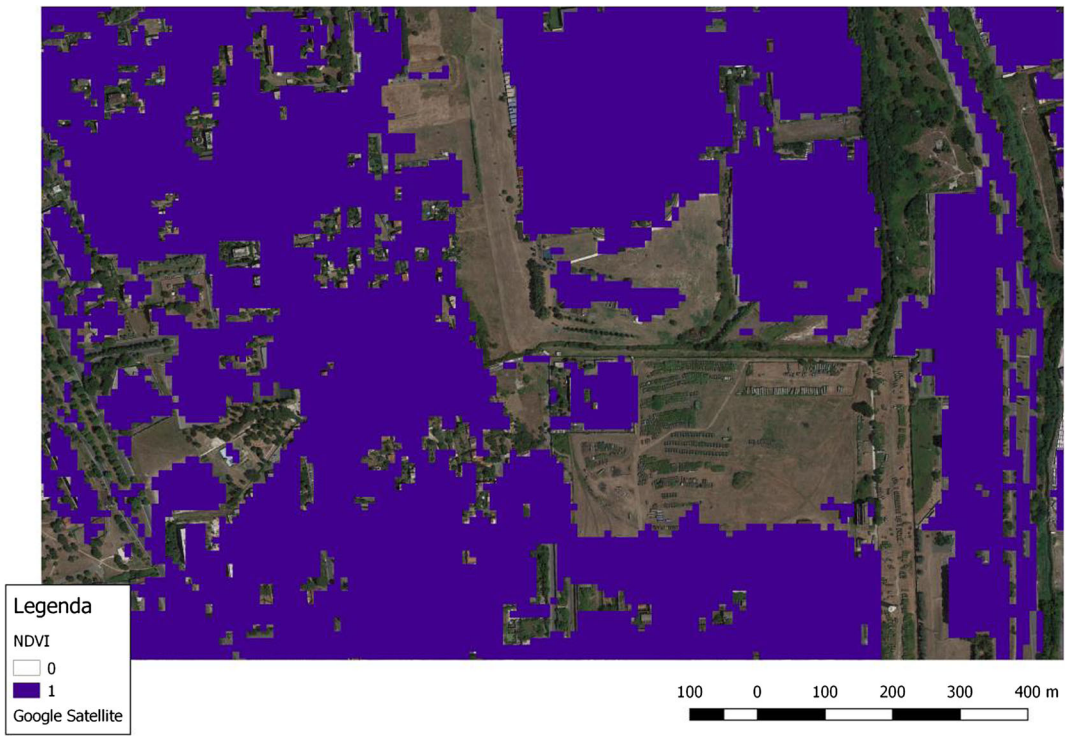

Fig. 25 NDVI map, Colle Prenestino–Rome. Code 1 indicates areas where the NDVI index is less than 0.4, whereas code 0 indicates areas in which the NDVI index is more than 0.4

Fig. 26 Filtered map of land consumption change, Colle Prenestino–Rome

for this study[3]), indicating areas where the vegetation is absent and the soil may be bare or built on. By contrast, code 0 indicates areas where the value of NDVI is above 0.4, meaning that there is a vegetation cover.

The overlap of the potential land consumption (from SAR data) and the NDVI-based map generated a new map, shown in Fig. 26, which represents the filtered map of land consumption.

Discussion and conclusions

This paper proposes an innovative method for monitoring land consumption through an automatic procedure that integrates SAR and optical data, and can be effectively used to generate land consumption maps or update existing ones. The main input of the procedure is a series of SAR amplitude images acquired over a given geographical area and observation period. The SAR data offer the advantage of all-weather, day and night image acquisition: they are suited to the analysis of areas frequently covered by clouds. The procedure makes use of a step detector based on a Bayesian approach. This approach is simple, unsupervised, and automatic, feasible for users who are not experts in the field. The optical data are used to derive an NDVI map, which is used to filter the SAR-based results. The proposed procedure detects the changes that have occurred as well as the time when they happened. In particular, it enables us to assess the evolution of artificial land cover over time and pinpoint the location of transformation of agricultural and natural areas into artificial areas (land consumption).

It is worth highlighting that this procedure assumes that a change causes an increase of the amplitude values (see Eq. 7). Consequently, changes are not detected whenever the new objects are characterized by low amplitude, such as a street, a square, or a set of solar panels.

This aspect could be improved in further research activities. Further research activity should also be devoted to a complete validation of the proposed procedure results.

The proposed method, based on the Bayesian approach for change detection, could be improved by implementing a more accurate and precise algorithm, e.g., a two-dimensional neural network (Lindblad and Kinser 2005). This algorithm should be able to recognize changes associated with low-amplitude values, which are currently not highlighted, and reduce false changes.

The implementation of the complete algorithm in the Google Earth Engine could represent an important further development. The Google Earth Engine archive includes historical images from 1990 to date, collects new images continuously, and provides many other useful tools for analyzing large sets of images. This platform could be particularly useful in the analysis of historical series of images or in the integration of optical data and radar, having such a vast catalog of data at hand (Landsat, Sentinel-1, MODIS, etc.).

Assessing the pace of growth of land consumption is important in light of the European objectives for 2020 (European Commission 2011) and the Roadmap to a Resource Efficient Europe (European Commission 2011b). Despite these important policy documents that aim to achieve zero net soil sealing by 2050, the delivery of guidelines of good practices to mitigate soil sealing (European Commission 2012) and the delivery of the United Nations agenda for sustainable development goals (goal 11: Make cities and human settlements inclusive, safe, resilient and sustainable, and goal 15: Sustainably manage forests, combat desertification, halt and reverse land degradation, halt biodiversity loss) (United Nations 2015), there are currently no signs of change in historical trends: land consumption continues to increase annually at the European and global levels (United Nations 2014; European Commission 2012). For instance, the increase of artificial cover areas was an ongoing process across the EU at the rate of 930 km^2/year in 2000–2006 and 845 km^2/year in 2006–2012. This represents a substantial amount of land often being taken from agriculture (European Commission 2012). At the local level, it is fundamental to monitor changes because of the environmental effects as well as economic and social externalities (Irwin and Bockstael 2004) caused by land consumption; and it is important to foster the development of effective policies for sustainability and adaptation to environmental change (Cardona et al. 2012).

Through the proposed procedure, it is possible to create a useful alerts system for public administrations to monitor the territory and associated externalities, and for the correct implementation of urban planning and track phenomena such as abusive building activity.

[3] This value was chosen considering the resolution of Sentinel-2. Lower values would have been too restrictive in identifying areas where the pixel is mixed (for example, building site areas with little grass).

This method could provide a new service, that does not exist today, to supply a timely alert to the public administration about changes in land use and land cover, which represent a worrisome threat for soil conservation and related services provided as support for human well-being. Thanks to the frequent revisiting of ESA Sentinel data, we will be able to monitor soil consumption in a new, innovative, and rapid way (e.g., even on a monthly basis, depending on the phenomena in action), thus offering an effective support for future sustainable land use management at multiple scales (from municipal, to provincial, regional, and national levels). Customers could be public administrations, mainly at the local level, as they are in charge of operational tasks to favor soil protection, among them municipalities, regions, park authorities, protected areas agencies, and basin authorities.

In the Italian context, the Italian Parliament is currently debating a law to limit land consumption, considering the main objective of no net land take by 2050 (European Commission 2011b). To meet the objective, the Italian National Institute for Environmental Protection and Research (ISPRA) recently published the National Report on Land Consumption based on the mapping of land consumption through photointerpretation and semi-automatic classification of optical images (ISPRA 2017). It is often difficult to update land consumption maps using only optical images. For this reason, in addition to the above proposed applications, the method developed in this paper could be applied in order to improve the mapping of land consumption by ISPRA using SAR images, overcoming the issue of cloud cover, time spent using photointerpretation methods, and increasing the frequency of map updates.

Compliance with ethical standards

Conflict of interest The authors declare that they have no conflict of interest.

References

Angelis, C. F., Freitas, C. C., Valeriano, D. M., & Dutra, L. V. (2002). Multitemporal analysis of land use/land cover JERS-1 backscatter in the Brazilian tropical rainforest. *International Journal of Remote Sensing, 23*(7), 1231–1240.

As-syakur, A. R., Wayan Sandi Adnyana, I., Wayan Arthana, I., & Wayan Nuarsa, I. (2012). Enhanced built-up and bareness index (EBBI) for mapping built-up and bare land in an urban area. *Remote Sensing, 4*, 2957–2970.

Brook R. M. and D ávila J. (2000). The peri-urban interface: a tale of two cities. Gwynedd, Wales: School of Agricultural and Forest Sciences, University of Wales and Development Planning.

Campbell J.B., Wynne R.H. (2011). Introduction to remote sensing. Guilford Press, 667pp.

Cardona, O.D., M.K. van Aalst, J. Birkmann, M. Fordham, G. McGregor, R. Perez, R.S. Pulwarty, E.L.F. Schipper, and B.T. Sinh (2012). Determinants of risk: exposure and vulnerability. In: Managing the risks of extreme events and disasters to advance climate change adaptation [Field, C.B., V. Barros, T.F. Stocker, D. Qin, D.J. Dokken, K.L. Ebi, M.D. Mastrandrea, K.J. Mach, G.-K. Plattner, S.K. Allen, M. Tignor, and P.M. Midgley (eds.)]. A Special Report of Working Groups I and II of the Intergovernmental Panel on Climate Change (IPCC). Cambridge University Press, Cambridge, UK, and New York, NY, USA, pp. 65–108.

Congedo L., Marinosci I., Riitano N., Strollo A., De Fioravante P., Munafò M. (2017). Monitoring of land consumption: an analysis of loss of natural and agricultural areas in Italy. Annali di Botanica, 7: 1–9.

CRCS. (2012). *Rapporto 2012. Centro di Ricerca sui Consumi di Suolo*. Milano: INU Edizioni.

EEA, European Environment Agency (2011). Urban soil sealing in Europe. https://www.eea.europa.eu/articles/urban-soil-sealing-in-europe.

Estoquea, R. C., Murayamaa, Y., & Akiyamab, C. M. (2015). Pixel-based and object-based classifications using high- and medium-spatial-resolution imageries in the urban and suburban landscapes. *Geocarto International, 30*(10), 1113–1129.

European Commission (2011). Our life insurance, our natural capital: an EU biodiversity strategy to 2020. COM (2011) 244 final. Brussels.

European Commission (2011b). Roadmap to a resource efficient Europe. COM (2011)571 final. Brussels.

European Commission (2012). Guidelines on best practice to limit, mitigate or compensate soil sealing. SWD (2012) 101. Brussels.

Fan, F., Weng, Q., & Wang, Y. (2007). Land use and land cover change in Guangzhou, China, from 1998 to 2003, based on Landsat TM/ETM+ imagery. *Sensors, 7*, 1323–1342.

Gómez, C., White, J., & Wulder, M. (2016). Optical remotely sensed time series data for land cover classification: a review. *ISPR Journal of Photogrammetry and Remote Sensing, 116*(June 2016), 55–72.

Gomez-Chova, L., Fernández-Prieto, D., Calpe, J., Soria, E., Vila, J., & Camps-Valls, G. (2006). Urban monitoring using multitemporal SAR and multi-spectral data. *Pattern Recognition Letters, 27*(4), 234–243.

Gorelick, N., Hancher, M., Dixon, M., Ilyushchenko, S., Thau, D., & Moore, R. (2017). Google Earth Engine: planetary-scale geospatial analysis for everyone. *Remote Sensing of Environment, 202*, 18–27.

Huber S., Prokop G., Arrouays D., Banko G. et al. (2008). Environmental assessment of soil for monitoring. Volume I indicators and criteria. JRC, Office for the Official Publications of the European Communities.

Irwin, E. G., & Bockstael, N. E. (2004). Land use externalities, open space preservation, and urban sprawl. *Regional Science and Urban Economics, 34*(6), 705–725.

ISPRA, Istituto Superiore per la Protezione e Ricerca Ambientale (2017). Consumo di suolo, dinamiche territoriali e servizi ecosistemici. Edizione 2017. (In Italian).

Lam N. SN. (2008). Methodologies for mapping land cover/land use and its change. Advances in land remote sensing. Springer, pp 341–367.

Lindblad T., Kinser J.M. (2005). Image processing using pulse-coupled neural networks, Second, Revised Version, 169pp.

Maes, J., Egoha, B., Willemen, L., et al. (2012). Mapping ecosystem services for policy support and decision making in the European Union. *Ecosystem Services, 1*, 31–39.

Moran, M. S., Hymer, D. C., Qi, J., & Kerr, Y. (2002). Comparison of ERS-2 SAR and Landsat TM imagery for monitoring agricultural crop and soil conditions. *Remote Sensing of Environment, 79*(2), 243–252.

Munafò M., Riitano N. (2016). Cause ed effetti del consumo di suolo. Consumo di suolo, dinamiche territoriali e servizi ecosistemici. Ed. 2016, pp. 4–6 (in Italian).

Munafò M., Marinosci I., Congedo L., La Mantia C., Luti T., Marchetti M., Raudner A., Riitano N., Sallustio L., Strollo A. (2016). Monitoraggio del territorio e del consumo di suolo in Italia. Consumo di suolo, dinamiche territoriali e servizi ecosistemici. Ed. 2016, pp. 23–26 (in Italian).

O'Ruanaidh J.J.K., Fitzgerald W.J. (1996). Numerical Bayesian methods applied to signal processing. Springer, 244pp.

Patel, N., Angiuli, E., Gamba, P., Gaughan, A., Stevens, F., Tatem, A., & Trianni, G. (2015). Multitemporal settlement and population mapping from Landsat using Google Earth Engine. *International Journal of Applied Earth Observation and Geoinformation, 35*(Part B), 199–208.

Poursanidis, D., & Chrysoulakis, N. (2017). Remote sensing, natural hazards and the contribution of ESA Sentinels missions. *Remote Sensing Applications: Society and Environment, Volume, 6*(April 2017), 25–38.

Satalino G., Balenzano M.F., Belmonte A. and Impedovo D. (2011). Land cover classification by using multi-temporal COSMO-SkyMed data. 2011 6th International Workshop on the Analysis of Multi-temporal Remote Sensing Images (Multi-Temp).

Scalenghe R., Ajmone Marsan F. (2009). The anthropogenic sealing of soil in urban areas. Landscape and urban planning, Volume 90, Issues 1-2**,** 15 March 2009, Pages 1–10.

Sun, Z., Wang, C., Guo, H., & Shang, R. (2017). A modified normalized difference impervious surface index (MNDISI) for automatic urban mapping from Landsat imagery. *Remote Sensing, 9*, 942.

United Nations (2014). World urbanization prospects, the 2014 revision. Final report, ST/ESA/SER.A/366, New York.

United Nations (2015). Transforming our world: the 2030 agenda for sustainable development. A/RES/70/1, UN General Assembly, 21 October, 2015.

Yousif O., Ban Y. (2015). Object-based urban change detection using high resolution SAR images. 2015 Joint Urban Remote Sensing Event (JURSE).

Zhang X., Tang X., Gao X., Zhao H. (2018). Multitemporal soil moisture retrieval over bare agricultural areas by means of alpha model with multisensor SAR data. Advances in Meteorology, Volume 2018, Article ID 7914581, 17 pages.

Zhu, Z., Woodcock, C. E., Rogan, J., & Kellndorfer, J. (2012). Assessment of spectral, polarimetric, temporal, and spatial dimensions for urban and peri-urban land cover classification using Landsat and SAR data. *Remote Sensing of Environment, 117*, 72–82.